# *Effective elastic properties of periodic hexagonal honeycombs*



**Citation:** Malek, Sardar, and Gibson, Lorna. "Effective Elastic Properties of Periodic Hexagonal Honeycombs." Mechanics of Materials 91 (December 2015): 226–240 © 2015 Elsevier Ltd

**As Published:** http://dx.doi.org/10.1016/j.mechmat.2015.07.008

**Publisher:** Elsevier

**Persistent URL:** http://hdl.handle.net/1721.1/112341

**Version:** Author's final manuscript: final author's manuscript post peer review, without publisher's formatting or copy editing

# Effective Elastic Properties of Periodic Hexagonal Honeycombs

Sardar Malek and Lorna Gibson*

Department of Materials Science and Engineering
Massachusetts Institute of Technology
77 Massachusetts Ave, Cambridge, MA, USA 02139

## Abstract

We investigate the elastic behaviour of periodic hexagonal honeycombs over a wide range of relative densities and cell geometries, using both analytical and numerical approaches. Previous modelling approaches are reviewed and their limitations identified. More accurate estimates of all nine elastic constants are obtained by modifying the analysis of Gibson and Ashby (1997) to account for the nodes at the intersection of the vertical and inclined members. The effect of the nodes becomes significant at high relative densities. We then compare the new analytical equations with previous analytical models, with a numerical analysis based on a computational homogenization technique and with data for rubber honeycombs over a wide range of relative densities and cell geometries. The comparisons show that both the new analytical equations and numerical solutions give a remarkably good description of the data. The results provide new insights into understanding the mechanics of honeycombs and designing new cellular materials in the future.

## Keywords

Honeycomb, Homogenization, Effective Properties, Modelling, Finite Element Method, Unit cell

* Corresponding author, email: ljgibson@mit.edu

# 1 Introduction

Honeycombs are widely used as the cores of sandwich panels in the aerospace, automotive, construction, marine and wind energy industries. The separation of stiff, strong faces (for instance, fiber reinforced composite laminates) by a lightweight, typically cellular core, increases the moment of inertia of the panels with little increase in weight, making them efficient for resisting bending and buckling loads.

Honeycombs are used extensively in the aerospace industry, due to their high specific stiffness and strength (Burton and Noor, 1997). The response of a sandwich structure under different types of load depends, in part, on the effective (equivalent) properties of the core (Allen, 1969; Burton and Noor, 1997; Hohe and Becker, 2001; Balawi and Abot, 2008). As a result, the effective elastic and inelastic properties of honeycombs have been widely studied using analytical and numerical models (e.g. (Kelsey et al., 1958; Gibson et al., 1982; Gibson and Ashby, 1988, 1997; Zhang and Ashby, 1992; Burton and Noor, 1997; Simone and Gibson, 1998; Balawi and Abot, 2008)). Many of these models use approximations that limit their validity to low values of the ratio of cell wall thickness to length and to isotropic cell walls. With a view towards applying honeycomb models to natural materials such as balsa wood, with relatively high values of cell wall thickness to length (compared with engineering honeycombs) and with anisotropic cell walls, we extend Gibson and Ashby's honeycomb model.

We first review some widely used models available in the literature and identify the limitations of these models in Section 2. The analysis of Gibson and Ashby (1997) for hexagonal honeycombs with constant cell wall thickness is extended in Section 3 to allow more accurate estimates of all nine elastic constants of honeycombs with cell walls of constant thickness. In addition, new analytical equations for the elastic constants of honeycombs with double thickness vertical cell walls are presented in Appendix A.

A 3D numerical analysis for the elastic constants, based on a computational homogenization technique, is described in Section 4. It is intended that the numerical model provide reference solutions to examine the range of validity of the new analytical equations. In addition, both the analytical and numerical results are compared with experimental data on rubber honeycombs (Gibson, 1981) in Section 5.

Both the new analytical results and the numerical results give a remarkably good description of the available experimental data. The numerical approach can easily be adapted for an orthotropic cell wall, as in the case of woods. Finally, the use of the numerical approach in investigating the effect of relative density and cell geometry on the effective elastic properties of honeycombs and understanding the mechanics of honeycombs is discussed in Section 6.

# 2 Literature

One of the most widely used models for the elastic constants of honeycombs is that of Gibson and Ashby and co-workers (Gibson et al., 1982; Gibson and Ashby, 1988, 1997). Their initial studies of the in-plane moduli focussed on bending deformation in cell walls of uniform thickness; bending-based models give a good description of the elastic moduli of low relative density honeycombs. They also modeled the out-of-plane elastic moduli. In general, good agreement between the models and experimental results was reported for all properties, although some discrepancies were observed, especially for in-plane shear properties which were attributed to shear deformation in the testing jig. Later on, they extended the models to include the

contribution of axial and shear deformations to the in-plane moduli and to include honeycombs with vertical walls of double thickness, representative of many honeycombs made by the corrugation and expansion processes (Gibson and Ashby, 1997).

Honeycombs with double thickness vertical cell walls have attracted more attention in the literature than those with constant cell wall thickness. Masters and Evans (1997) derived analytical equations for the effective in-plane elastic properties of honeycombs with double thickness vertical cell walls, considering axial, bending and shear deformations as well as hinging (change of the angle at the intersection of vertical and inclined walls), obtaining results similar to those of Gibson and Ashby (Gibson and Ashby, 1997). The full set of analytical equations for honeycombs were also given by Burton and Noor (1997) by incorporating a coefficient in the equations derived by Gibson and Ashby (1988).

There are several limitations to the above models. An exact expression for one of the out-of-plane shear moduli is not obtained; only upper and lower bounds. The accuracy of the in-plane models accounting for shear and axial deformation of the cell walls was never fully investigated. Although the analytical models given by Gibson and Ashby (1997) and Masters and Evans (1997) are similar and predict the effective elastic properties of low relative density honeycombs well, they become less accurate with increasing relative density. In addition, the analytical models do not capture the slight in-plane anisotropy of double wall honeycombs which increases with relative density.

Numerical analysis has proven to be a powerful and promising approach, once validated, in studying the mechanics of heterogeneous media in the past (Guedes and Kikuchi, 1990; Kanit et al., 2006; Malekmohammadi, 2014). Therefore, some researchers have used numerical approaches (e.g. FE based) to better understand and predict the elastic behaviour of honeycombs (Chamis et al., 1988; Grediac, 1993; Silva et al., 1995; Vougiouka et al., 1998; Guo and Gibson, 1999; Meraghni et al., 1999; Hohe and Becker, 2001; Chen, 2011; Catapano and Montemurro, 2014). However, only few of them (Vougiouka et al., 1998; Hohe and Becker, 2001; Chen, 2011; Catapano and Montemurro, 2014), have actually attempted to predict all the elastic constants for generally orthotropic honeycombs and compare them with available analytical estimates or experimental data. Most researchers, employed shell (Chamis et al., 1988; Grediac, 1993; Vougiouka et al., 1998; Meraghni et al., 1999; Hohe and Becker, 2001; Chen, 2011) or beam (Silva et al., 1995; Guo and Gibson, 1999) elements for their numerical models. It should be noted that the 3D cell geometry and features such as the size of nodes at the intersection of the vertical and inclined members are not fully captured using shell elements. Moreover, most shell elements have limitations in capturing the true variation of normal and shear stresses through the shell thickness. As pointed out by Catapano and Montemurro (2014), this makes the validity of these numerical models questionable, especially for honeycombs with thick cell walls.

Recently, Catapano and Montemurro (2014) conducted a 3D numerical study on the effective elastic properties of honeycombs with double thickness cell walls using the finite element method with solid elements. Predictions were compared with analytical models presented in Burton and Noor (1997) and Grediac (1993) for honeycombs with double thickness vertical walls. For in-plane properties, relative errors ranging from 8 to 23.5% were reported between shell-based models and solid-based models, although no significant difference was reported for out-of-plane properties. These differences for in-plane properties were attributed to the presence of normal out-of-plane stresses in cell walls of honeycombs. However, no comparisons with experimental data were given to support this argument.

# 3 Analytical Approach

The models of Gibson and Ashby and co-workers (1981, 1982, 1988, 1997), ignore the vertices or nodes at the intersection of the vertical and inclined members of the periodic hexagonal honeycomb. While the effect of the nodes on the elastic moduli is negligible for low relative density honeycombs, it can be significant at higher relative densities. In this section, we modify Gibson and Ashby's equations by considering the nodes and introducing the effective bending length of the cell wall into the analysis. The results presented in this section are for honeycombs with uniform cell wall thickness; results for honeycombs with double thickness vertical cell walls are given in Appendix A.

We first calculate the relative density of periodic hexagonal honeycombs. As shown in Fig. 1, we note that the lengths of the inclined and vertical cell walls ($l_b$ and $h_b$, respectively) which can bend under in-plane loading are:

$$l_b = l - t/(2\cos\theta), \quad h_b = h - t(1-\sin\theta)/\cos\theta \tag{1}$$

where $t$ is the cell wall thickness and $\theta$ is the angle between the horizontal and the inclined cell wall, as shown in Fig. 1. The relative density for a unit cell of the material (shown in Fig. 2) can be determined by subtracting the void area within the cells:

$$\left(\frac{\rho^*}{\rho_s}\right) = \left(1 - \frac{A_{void}}{A_{cell}}\right) = \left(1 - \frac{l_b\left(h_b + l_b\sin\theta\right)}{l\left(h + l\sin\theta\right)}\right) \tag{2}$$

The out-of-plane Young's modulus of honeycombs in the axial or $X_3$ direction can be estimated by assuming that for the normal loading in the $X_3$ direction, the deformation is axial. Therefore, the longitudinal modulus of the honeycomb can be expressed as:

$$E_3^* = E_s\left(\frac{\rho^*}{\rho_s}\right) \tag{3}$$

The Young's moduli in the transverse, in-plane, directions (i.e. $X_1$ and $X_2$) are calculated as follows. In the $X_1$ direction, the modulus, $E_1^*$, can be obtained by dividing the applied stress to the induced strain:

$$E_1^* = \frac{\sigma_1}{\epsilon_1} \tag{4}$$

where

$$\sigma_1 = \frac{F_1}{b\left(h + l\sin\left(\theta\right)\right)} \tag{5}$$

and

$$\epsilon_1 = \frac{\delta_1}{l\cos\left(\theta\right)} \tag{6}$$

The applied force to each inclined member, $F_1$, and its resulting deflection in the $X_1$ direction, $\delta_1$, are shown in Fig. 3(b). Note that $b$ is the depth of the unit cell in Fig. 3(a). The total deflection, $\delta_1$, can be written as the sum of deflections due to the axial $\delta_a$, shear $\delta_s$, and bending $\delta_b$ deformation of the cell wall, in the $X_1$ direction (see Fig. 3):

$$\delta_1 = \delta_a \cos\theta + \delta_s \sin\theta + \delta_b \sin\theta \tag{7}$$

with:

$$\delta_a = \frac{F_1 l_b \cos\theta}{E_s b t} \tag{8}$$

$$\delta_s = \frac{F_1 {l_b}^3 \sin\theta}{12 E_s I}\left(2.4 + 1.5\nu_s\right)\left(\frac{t}{l_b}\right)^2 \tag{9}$$

$$\delta_b = \frac{F_1 {l_b}^3 \sin\theta}{12 E_s I} \tag{10}$$

It should be noted that in deriving the above equations, deformations within the node have been neglected. The shear deflection in Eq. (9) is calculated according to the Timoshenko beam theory (Timoshenko and Goodier, 1970).

The Young's modulus in $X_1$ direction can now be obtained by substituting Eq. (7) in Eq. (6) and subsequently in Eq. (4):

$$E_1^* = E_s\left(\frac{t}{l_b}\right)^3 \frac{\cos\theta}{\left(h/l + \sin\theta\right)\sin^2\theta}\left[\frac{1}{1+\left(2.4+1.5\nu_s+\cot^2\theta\right)\left(\frac{t}{l_b}\right)^2}\right] \tag{11}$$

Using a similar approach in the $X_2$ direction, the modulus $E_2^*$ is:

$$E_2^* = E_s\left(\frac{t}{l_b}\right)^3 \frac{\left(h/l + \sin\theta\right)}{\cos^3\theta}\left[\frac{1}{1+\left(2.4+1.5\nu_s+\tan^2\theta+\frac{2\left(h_b/l_b\right)}{\cos^2\theta}\right)\left(\frac{t}{l_b}\right)^2}\right] \tag{12}$$

The effective Poisson's ratios, $\nu_{12}^*$ and $\nu_{21}^*$ are calculated by considering the strains in different directions. For loading in the $X_1$ direction:

$$\nu_{12}^* = -\frac{\epsilon_{22}}{\epsilon_{11}} = -\frac{\frac{-\delta_2}{\left(h + l\sin\theta\right)}}{\frac{\delta_1}{l\cos\theta}} = \frac{\cos^2\theta}{\left(h/l+\sin\theta\right)\sin\theta}\left[\frac{1+\left(1.4+1.5\nu_s\right)\left(\frac{t}{l_b}\right)^2}{1+\left(2.4+1.5\nu_s+\cot^2\theta\right)\left(\frac{t}{l_b}\right)^2}\right] \tag{13}$$

where $\nu_s$ is the Poisson's ratio of the solid cell wall material. Note that it can be shown that the deflection in the transverse direction, denoted by $\delta_2$, is created by the axial, shear and bending deformation of the inclined member (see Fig. 3) as follows:

$$\delta_2 = -\delta_a \sin\theta + \delta_s \cos\theta + \delta_b \cos\theta \tag{14}$$

A similar analysis can be performed for loading in the $X_2$ direction. The final expression for $\nu_{21}^*$ is:

$$\nu_{21}^* = \frac{\sin\theta\left(h/l + \sin\theta\right)}{\cos^2\theta}\left[\frac{1+\left(1.4+1.5\nu_s\right)\left(\frac{t}{l_b}\right)^2}{1+\left(2.4+1.5\nu_s+\tan^2\theta+\frac{2\left(h_b/l_b\right)}{\cos^2\theta}\right)\left(\frac{t}{l_b}\right)^2}\right] \tag{15}$$

In order to calculate the in-plane shear modulus, the shear force $F$ applied to a vertical member gives a shear stress $\tau_{12}$ of (Fig.4):

$$\tau_{12} = \frac{F}{2bl\cos\theta} \tag{16}$$

As shown in Fig. 4(b), the applied in-plane shear force to the unit cell, $F$, is carried by two inclined members equally. Note that equilibrium requires:

$$S = \frac{F(h + l\sin\theta)}{2l\cos\theta} \tag{17}$$

The effective in-plane shear modulus $G_{12}^*$ can be calculated as:

$$G_{12}^* = \frac{\tau_{12}}{\gamma_{12}} = \frac{\tau_{12}}{\gamma_h + \gamma_l} \tag{18}$$

The total strain $\gamma_{12}$ in Eq. (18) is composed of the shear strain due to deflection in the vertical $\gamma_h$ and the inclined members, $\gamma_l$, respectively. The shear strain in the vertical member is calculated to be:

$$\gamma_h = \frac{u_h}{\frac{\left(h + l\sin\theta\right)}{2}} = \frac{Fh_b^2}{24E_sI}\left(\frac{l_b}{l}\right)\frac{1}{\left(h/l+\sin\theta\right)}\left[1+2\left(\frac{h_b}{l_b}\right)+2\left(\frac{h_b}{l_b}\right)\left(2.4+1.5\nu_s\right)\left(\frac{t}{h_b}\right)^2\right] \tag{19}$$

where $u_h$ is the displacement of the vertical member in the $X_1$ direction due to its rotation ($\phi$), bending and shear deformations (see Fig. 5(b)):

$$u_h = \frac{Fh_b^2}{48E_sI}\left[l_b + 2h_b + 2h_b\left(2.4+1.5\nu_s\right)\left(\frac{t}{h_b}\right)^2\right] \tag{20}$$

The shear strain in the inclined member, $\gamma_l$, is calculated as:

$$\gamma_l = \frac{2\left[\left(u_l\right)_{axial}\sin\theta + \left(u_l\right)_{shear}\cos\theta\right]}{l\cos\theta} \tag{21}$$

The first and second term in the numerator of Eq. (21) is the displacement of the inclined member due to the axial deformation, denoted by $\left(u_l\right)_{axial}$, and the shear deformation, denoted by $\left(u_l\right)_{shear}$, projected in the $X_2$ direction, respectively. These displacements are shown in Fig. 5 and are calculated as:

$$\left(u_l\right)_{axial} = \frac{Fl_b\cos\theta}{4E_s bt} + \frac{Sl_b\sin\theta}{2E_s bt} \tag{22}$$

$$\left(u_l\right)_{shear} = \frac{Fh_b^{\,2}}{48E_s I}\frac{l_b}{\left(h_b/l_b\right)}\left(2.4+1.5\nu_s\right)\left(\frac{t}{l_b}\right)^2 \tag{23}$$

Substituting Eqs. (16), (19) and (21) into Eq. (18) and some simplifications gives:

$$G_{12}^{*} = E_s\left(\frac{t}{l_b}\right)^3 \frac{\left(h/l+\sin\theta\right)}{\left(\frac{h_b}{l_b}\right)^2\cos\theta}\left(\frac{1}{C}\right) \tag{24}$$

where $C$ is expressed as:

$$C = \left[1+2\left(h_b/l_b\right)+\left(\frac{t}{l_b}\right)^2\left(\frac{\left(2.4+1.5\nu_s\right)}{h_b/l_b}\left(2+\left(\frac{h}{l}\right)+\sin\theta\right)+\frac{h/l+\sin\theta}{\left(\frac{h_b}{l_b}\right)^2}\left[\left(h/l+\sin\theta\right)\tan^2\theta+\sin\theta\right]\right)\right] \tag{25}$$

The above equations are similar to those given in Appendix 4B of Gibson and Ashby (1997). However, there are slight differences in expressing terms which involve the length of inclined and vertical members of the honeycomb structure, as a result of considering the area of the nodes in the current analysis. As shown in Section 5.2, this more accurate analysis results in improved predictions of the honeycomb moduli.

Upper and lower bounds for the out-of-plane shear moduli were obtained by previous researchers (Kelsey et al., 1958; Gibson et al., 1982; Gibson and Ashby, 1988, 1997). However, by considering compatibility of the displacement and traction at the interface of multiple blocks of the material unit cell (see Fig. 6) as well as equilibrium of forces, we obtain closed-form equations:

$$G_{13}^{*} = G_s\left(\frac{t/l}{\left(h/l+\sin\theta\right)\cos\theta}\right)\left[\cos^2\theta\left(\frac{l_b}{l}\right)+\frac{3}{4}\left(\frac{t}{l}\right)\tan\theta-\frac{\cos\theta}{2}\left(\frac{t}{l}\right)\left(2\sin\theta-1\right)\right] \tag{26}$$

$$G_{23}^{*}=G_{s}\left(\frac{t/l}{\left(h/l+\sin\theta\right)\cos\theta}\right)\left[\sin^{2}\theta\left(\frac{l_{b}}{l}\right)+\frac{h_{b}}{2l}+\frac{3}{4}\left(\frac{t}{l}\right)\tan\theta-\frac{\sin^{2}\theta}{2\cos\theta}\left(\frac{t}{l}\right)\left(2\sin\theta-1\right)\right] \quad (27)$$

The analysis to obtain these equations is quite lengthy and therefore it is given in Appendix B for reference.

The effective out-of-plane Poisson's ratios are equal to those of the solid cell wall material, i.e.:

$$\nu_{31}^{*}=\nu_{32}^{*}=\nu_{s} \quad (28)$$

The validity of this estimate is examined below using finite element reference solutions.

It is noted that once the effective Young's moduli in all three different directions (i.e. $E_{1}^{*}$, $E_{2}^{*}$ and $E_{3}^{*}$) are determined, the other effective Poisson's ratio can be found from the reciprocal relations:

$$\nu_{13}^{*}=\frac{E_{1}^{*}}{E_{3}^{*}}\nu_{31}^{*},\quad \nu_{23}^{*}=\frac{E_{2}^{*}}{E_{3}^{*}}\nu_{32}^{*} \quad (29)$$

# 4 Numerical Approach

Numerical reference solutions are obtained using a computational homogenization technique based on full-field microstructural simulations. Computational homogenization is a powerful technique in finding the effective properties of heterogeneous materials (Guedes and Kikuchi, 1990; Kanit et al., 2006). This method is versatile and has been used for estimating the effective properties of heterogeneous materials with complex morphological characteristics (e.g. (Moulinec and Suquet, 1998; Michel et al., 1999)). Using computational homogenization, the effective stiffness tensor is determined by solving six elementary boundary value problems corresponding to three uniaxial extensions and three simple shear loadings (see (Gereke et al., 2012)).

Previous studies have shown that the apparent stiffness tensor of a given volume of the material depends on the type of boundary conditions applied (Huet, 1990; Kanit et al., 2003; Xia et al., 2003). It has been shown that periodic boundary conditions are ideally suited for both periodic and random media (Kanit et al., 2003, 2006; Xia et al., 2003). Independent of the size of the volume, the apparent elastic properties obtained with periodic boundary conditions are closer to the effective properties than with other boundary conditions (i.e. homogeneous strain or stress boundary conditions). Therefore, a numerical approach based on a computational homogenization technique with periodic boundary conditions is used here to provide reference solutions and evaluate the analytical models in this paper.

## 4.1 Unit Cell

The hexagonal honeycomb is assumed to have a periodic microstructure with constant wall thickness; a unit cell can be identified (see Fig. 2). To investigate the effect of the relative density and cell geometry on the effective properties of the honeycomb, the cell wall lengths $l$ and $h$, thickness, $t$, and the angle $\theta$ are all defined as parameters that can be varied.

As stated by Catapano and Montemurro (2014), only solid elements capture the correct stress and strain distribution in the cell walls of 3D honeycombs. Therefore, the unit cell depicted in Fig. 7 is discretized using 8-node linear brick elements, C3D8I, in ABAQUS© software (ABAQUS Inc., 2013). The unit cell is discretized in a general way such that it can be used for multi-scale modelling of different wood species in future studies, similar to Qing and Mishnaevsky (2009) and Gereke et al. (2011). The cell wall of different wood species consists of four different layers (i.e. S1, S2, S3, CML). Therefore, four layers with distinct material behaviour are implemented for the cell walls. The material behaviour of each layer is defined as generally orthotropic and elastic. For this study, equal isotropic properties are assigned to all layers.

### 4.2 Stiffness Matrix Computation

The effective stiffness $\overline{C}$ of the honeycomb with the linear elastic cell wall material is defined by:

$$\overline{\sigma} = \overline{C} : \bar{\epsilon} \tag{30}$$

In the above equation, $\overline{\sigma}$ and $\bar{\epsilon}$ are the volume average of the stress and strain tensors in the unit cell, respectively. To determine the effective stiffness matrix of a unit cell of the material, denoted by $\overline{C}$, six elementary loadings (three uniaxial extensions and three simple shear loadings) corresponding to pre-specified forms of the average strain tensor $\bar{\epsilon}$ have to be successively applied to the unit cell. In each case, the local problem is solved by the finite element method.

The volume average of the resulting stress field in the unit cell, denoted by $\overline{\sigma}$, provides a specific column of the stiffness tensor (6×6 matrix representation), see e.g. Kanit et al., 2006 for more details. The engineering constants are then determined from the components of the compliance matrix obtained by taking the inverse of the stiffness matrix.

### 4.3 Boundary Conditions

To model the true behaviour of periodic honeycombs, just like any other periodic media (e.g. unidirectional composites), periodicity of displacements and tractions on the boundaries are required. Applying periodic boundary conditions instead of homogeneous displacement or traction boundary conditions prevents any over-constrained conditions in the numerical model and results in more accurate predictions of effective properties (Xia et al., 2003).

Kinematical periodic boundary conditions are prescribed to impose each of the six elementary loadings. For a given load (corresponding to a prescribed strain $\varepsilon$), the displacement field, $u(x)$ for any point $x$ belonging to the boundary $\partial\Omega$ of the unit cell $\Omega$ must be periodic (see (Malekmohammadi, 2014)). To apply periodic boundary conditions, for every pair of opposite points $A$ and $B$ on the boundary of unit cell, $\partial\Omega$, the following relation has been imposed:

$$u(x_B) - u(x_A) = \varepsilon.(x_B - x_A); \quad \forall x \in \partial\Omega \tag{30}$$

where $x_A$ and $x_A$ are the coordinates of the two opposite points. The periodic boundary conditions ensure the following average relationship:

$$\bar{\epsilon} = \langle \epsilon(x) \rangle = \frac{1}{V_\Omega} \int_\Omega \epsilon(x) dV \tag{31}$$

where $\varepsilon(x)$ is the strain field in the unit cell and $V_\Omega$ is the total volume of the unit cell $\Omega$.

Periodic boundary conditions are implemented in ABAQUS© software (ABAQUS Inc., 2013) using Python© scripts (Python, 2013). Python scripts are used to create geometries, generate lists of nodes and elements, and define material properties in an appropriate format as required to be employed in the ABAQUS© environment. The resulting stress and strain fields are used to calculate the average stress and strain tensors and hence the effective stiffness matrix for the unit cell of the honeycomb is calculated.

### 4.4 Convergence

To determine the suitable mesh size for the discretized model, a convergence study is performed employing different mesh sizes. According to this study, a mesh size of 40 × 8 × 3 (i.e. number of elements along each cell wall length × thickness × depth) provides converged values for all engineering elastic constants. The results of this study for elastic properties are shown in Fig. 8. Different ABAQUS © shell (S4 and S4R) and solid (C3D8, C3D8R and C3D8I) elements were examined for this study. The reduced-integration linear elements (S4R and C3D8R) converged rapidly as the mesh was refined. However, the elements require hourglass control (see (ABAQUS Inc., 2013)) which is out of the scope of this study.

It was found that regular 3D elements (C3D8), do not lead to converged values even with reasonably fine meshes. This is due to the shear locking of solid elements in bending which leads to unrealistically stiff results. Shear locking occurs in fully integrated, first order interpolation elements (e.g. C3D8) subjected to bending due to their numerical formulation and the induced unrealistic shear strains (see (Wang et al., 2000; Bower, 2010)). To overcome this problem, incompatible mode elements (C3D8I) were used. In these elements, in addition to the displacement degrees of freedom, incompatible deformation modes have been incorporated in the element formulation (ABAQUS Inc., 2013).

The results of 4-node shell elements (S4 and S4R) matched those of solid C3D8I element for honeycombs with thinner cell walls. As the cell wall thickness increased, the shell element results deviated from the solid elements results. This is due to inaccuracy of these shell elements in describing the variation of through-thickness stresses in thick cell walls (Catapano and Montemurro, 2014). Therefore, only numerical results obtained using C3D8I elements are reported in this paper.

## 5 Validation

### 5.1 Experiments

Gibson (1981) conducted a detailed experimental study on the mechanical properties of silicone rubber honeycombs with varying ratios of cell wall thickness to length, $t/l$, and cell geometry ( $h/l$ and $\theta$); each honeycomb had constant cell wall thickness. The results of this previous study are used to assess the accuracy of both the analytical and numerical approaches described in this paper. Briefly, specimens were prepared by mixing silicon rubber with a hardener and pouring the mixture into moulds of the appropriate geometry. Each sample was loaded uniaxially in

different directions and, separately, in shear in different planes. The in-plane moduli in the $X_1$ and $X_2$ directions, as well as the in-plane shear modulus, were all measured from the slope of load-deflection curves. The in-plane Poisson's ratios, $\nu_{12}$ and $\nu_{21}$ of the honeycombs were also determined by displacement measurements in two perpendicular directions when samples were loaded uniaxially in the $X_1$ and $X_2$ directions.

Gibson and Ashby (1997) found that their analytical model predictions gave a good description of their experimental measurements for the in-plane properties of honeycombs. They concluded that the in-plane behavior of honeycombs is mainly governed by beam bending of cell walls. However, some discrepancies were also reported, especially for in-plane shear modulus where the analytical model predictions were lower than the experimental values for all samples. The stiffening effect of the shear jig was reported as the possible reason for the discrepancies. As we show in the following section, numerical study by finite element method reveals that this may not be the only reason for the observed discrepancies.

### 5.2 Honeycombs with uniform cell wall thicknesses

Fig. 9 shows comparisons for the effective Young's moduli in the three directions. In the in-plane directions, the improved analytical model (Eqs. (11) and (12)) and the finite element results give an excellent description of the experimental measurements. Excellent agreement is also observed between the analytical estimates (Eq. (3)) and the numerical reference solutions for Young's modulus in the $X_3$ direction of honeycombs with various relative densities and cell geometries.

Comparisons between the analytical models ((Gibson and Ashby, 1997) and Eqs. (24), (26) and (27)) and numerical results for the effective shear moduli are given in Fig. 10. Experimental data for in-plane properties (Gibson, 1981) are also shown to investigate the validity of the numerical model and the accuracy of the analytical equation (Eq. (24)) in predicting in-plane shear modulus of these honeycombs. The results show that the estimates of Eq. (24) are closer to the effective in-plane shear moduli of regular honeycombs than those of previous equations presented in (Gibson and Ashby, 1997), especially at higher $t/l$ ratios.

Estimates for the in-plane Poisson's ratios (Eq. (13)) are also found to be closer to the measured Poisson's ratios than those obtained by previous equations (see Fig. 11). For the out-of-plane Poisson's ratios, i.e. $\nu_{32}$ and $\nu_{31}$, the numerical reference solutions indicates that the estimate of Eq. (28) is valid for the wide range of cell wall thickness to length ratios studied here (i.e. a constant value, $\nu_s$, not shown here). In general, the very good agreement between numerical and experimentally measured values for the in-plane properties of honeycombs validates the capabilities of current numerical approach in modelling the effective properties of periodic hexagonal honeycombs.

To better understand the role of nodes in transferring in-plane and out-of-plane loads, the distribution of stresses through the cell walls are examined in numerical simulations. For in-plane tensile loading in the $X_2$ direction, the axial stress distribution in the vertical and inclined cell wall members and nodes at their intersection is given in Fig. 12. Note that the stress distribution is given in the local coordinate systems indicated below each plot in this figure. The applied tensile load in the $X_2$ direction is mostly carried through the extension of the vertical

member (Fig. 12(a)) and the axial and bending deformation of the inclined members (see Fig. 12(b)).

For in-plane shear loading, the deformed shape and the induced normal stresses, $\sigma_{22}$, in the unit cell's global coordinate system, are given in Fig. 13. The stress distribution in the cell wall indicates that that the vertical member deflects only due to bending and shear deformation, as it was assumed in Section 3 for estimating the effective in-plane shear modulus. Note that the symmetric maximum and minimum values of $\sigma_{22}$ occurring at the intersecting node regions implies that no axial deformation is present in vertical members. Fig. 14 shows how the load is transferred through the cell wall for out-of-plane shear loadings of the honeycombs. For out-of plane shear loading in $X_1$-$X_3$ plane, the applied load is transferred through shear deformation of the inclined members as shown in Fig. 14(a). The very small $\tau_{13}$ values in vertical members indicates that these members do not have any significant role in transferring the out-of plane shear load applied in the $X_1$-$X_3$ plane. However, both vertical and inclined members are sheared significantly when the load is applied in the $X_2$-$X_3$ plane (see Fig. 14(b)). These observations support the analytical approach presented in Appendix B for estimating the out-of-plane shear moduli of periodic honeycombs.

### 5.3 Honeycombs with double thickness vertical cell walls

For honeycombs with double thickness vertical cell walls, the predictions of the current analytical approach (Eqs. (A.3)-(A.8)) are compared with those of Gibson and Ashby (1997) as well as experimental data (Hexcel Corporation, 1999; Karakoc and Freund, 2012) for both in-plane and out-of-plane moduli in Figs. 15 and 16, respectively. Although in Gibson and Ashby (1997) analytical equations are given for honeycombs with both constant cell walls and double thickness vertical cell walls considering the bending deformation of cell walls, the extended equations (in which axial, shear and bending deformation of the cell walls were taken into account) are only given for honeycombs with constant thickness cell walls. Therefore, predictions of the previous analytical equations (Gibson and Ashby, 1997), in which only cell wall bending was considered, are compared with those obtained from Eqs. (A.3)-(A.8).

Fig. 15 and 16 show that although axial, shear and bending deformations are considered in these new equations, their predictions are very close to the previous ones given in Gibson and Ashby (1997) except for $G_{23}$. To show the relative agreement between the predictions and experimental data, the relative error ($\bar{e}$) between the two, as well as the correlation coefficient ($r^2$), are calculated for both the equations in Gibson and Ashby (1997) and Eqs. (A.3)-(A.8). For $G_{23}$, the predictions of Eq. (A.8) are between the upper and lower estimates, and close to the upper bound (Kelsey et al., 1958; Gibson and Ashby, 1997). For other moduli, the predictions of and Eqs. (A.4)-(A.6) are slightly higher than those of Gibson and Ashby (1997). It should be pointed out that the relative density of available commercial honeycombs given in these figures are quite low ($\rho^*/\rho_s < 0.05$) and bending deformation is considered as the main deformation mechanism in in-plane loading of these honeycombs. Therefore, the two predictions of both analytical approaches are expected to be very close. This explains the very good agreement between the two models for the in-plane moduli.

Quantitative inspection of the predictions of the two in-plane Young's moduli, i.e. $E_1$ and $E_2$, reveals the in-plane anisotropy of regular hexagonal honeycombs (i.e. $h/l = 1, \theta = 30^\circ$). This might seem surprising as the equations in Gibson and Ashby (1997) give identical values for the two in-plane Young's moduli of regular honeycombs. As reported by Balawi and Abot (2008), regular hexagonal honeycombs show a higher value for $E_2$ comparing to $E_1$ at high relative densities. However, the difference between the two in-plane moduli is negligible for the commercial honeycombs having low relative densities. Further detailed experimental studies on such honeycombs with higher relative densities are required to investigate the validity range of Eqs. (A.4)-(A.8).

## 6 Conclusions

The mechanics of honeycombs with periodic structures are investigated using analytical and numerical approaches. For this purpose, the analytical models previously developed for honeycombs with very low relative densities are revisited and a more complete analysis is presented. To better understand the mechanics of honeycombs, we focused on honeycombs with constant cell wall thickness. However, honeycombs with double thickness cell walls are also addressed and analytical equations are presented for their effective moduli in Appendix A due to their importance in industrial applications.

To investigate the importance and the role of the nodes at the intersection of the inclined and vertical cell wall members in the load transfer mechanism, a three dimensional numerical study with solid elements is conducted on honeycombs with constant cell wall thickness. The predictive capability of the numerical approach is then validated using a set of experimental data previously reported in the literature (Gibson, 1981). The results demonstrate the ability of the numerical approach to capture the effect of geometrical parameters, such as cell wall length, thickness, and angle, on the effective engineering constants of honeycombs. Moreover, they validate the accuracy of the complete analytical equations presented in this paper. These equations can be employed for optimizing the geometrical parameters of honeycombs as well as minimum weight analysis of sandwich structures with honeycomb cores (e.g. see (Burton and Noor, 1997; Catapano and Montemurro, 2014)).

As shown in this paper, the numerical approach is a promising approach in studying the mechanics of periodic honeycombs over a wide range of relative densities and cell geometries. It is flexible and can be used for cellular solids with various geometrical characteristics (e.g. cell wall size and thickness) and different types of solid cell wall properties (i.e. isotropic, transversely isotropic or orthotropic). It should be noted that the microstructure of several natural cellular materials such as wood and bone is similar to honeycombs. Findings of the current work provide new insights into understanding the mechanics of these natural cellular materials and designing novel bio-inspired materials in the future.

## Appendix A Analytical Equations for Honeycombs with Double Thickness Vertical Walls

In this appendix, the effective moduli of honeycombs with double thickness vertical walls are presented. Note that the geometrical parameters are slightly different for these honeycombs (see Fig. A1).

$$l_b = l - t\tan\left(\frac{\pi}{4}-\frac{\theta}{2}\right); \quad h_b = h - t\tan\left(\frac{\pi}{4}-\frac{\theta}{2}\right) \tag{A.1}$$

$$\left(\frac{\rho^*}{\rho_s}\right) = \left(1 - \frac{l\cos\theta\left(h_b + l\sin\theta\right)}{\left(l\cos\theta + t\right)\left(h + l\sin\theta\right)}\right) \tag{A.2}$$

$$E_3^* = E_s\left(\frac{\rho^*}{\rho_s}\right) \tag{A.3}$$

$$E_1^* = E_s\left(\frac{t}{l_b}\right)^3 \frac{\cos\theta}{\left(h/l + \sin\theta\right)\sin^2\theta}\left[\frac{1}{1+\left(2.4+1.5\nu_s+\cot^2\theta\right)\left(\frac{t}{l_b}\right)^2}\right] \tag{A.4}$$

$$E_2^* = E_s\left(\frac{t}{l_b}\right)^3 \frac{\left(h/l+\sin\theta\right)}{\cos^3\theta}\left[\frac{1}{1+\left(2.4+1.5\nu_s+\tan^2\theta+\frac{\left(h_b/l_b\right)}{\cos^2\theta}\right)\left(\frac{t}{l_b}\right)^2}\right] \tag{A.5}$$

$$G_{12}^* = E_s\left(\frac{t}{l_b}\right)^3 \frac{\left(h/l+\sin\theta\right)}{\left(\frac{h_b}{l_b}\right)^2\cos\theta}\left(\frac{1}{C}\right);$$

$$C = \left[1 + 2\left(h_b/l_b\right) + \left(\frac{t}{l_b}\right)^2\left(\frac{\left(2.4+1.5\nu_s\right)}{h_b/l_b}\left(4+\left(\frac{h}{l}\right)+\sin\theta\right) + \frac{\left(h/l+\sin\theta\right)}{\left(\frac{h_b}{l_b}\right)^2}\left[\left(h/l+\sin\theta\right)\tan^2\theta+\sin\theta\right]\right)\right] \tag{A.6}$$

$$G_{13}^* = G_s\left(\frac{t/l}{\left(h/l+\sin\theta\right)\left(\cos\theta+t/l\right)}\right)\left[\cos^2\theta\left(\frac{l_b}{l}\right)+2\left(\frac{t}{l}\right)\tan\left(\frac{\pi}{4}-\frac{\theta}{2}\right)\right] \tag{A.7}$$

$$G_{23}^* = G_s\left(\frac{t/l}{\left(h/l+\sin\theta\right)\left(\cos\theta+t/l\right)}\right)\left[\sin^2\theta\left(\frac{l_b}{l}\right)+\frac{h}{l}+\left(\frac{t}{l}\right)\tan\left(\frac{\pi}{4}-\frac{\theta}{2}\right)\right] \tag{A.8}$$

## Appendix B Analytical Approach for the Out-of-plane Shear Moduli of Honeycombs with Uniform Cell Walls

In this appendix, we present an analytical approach to obtain the closed-form equations for estimating the out-of-plane shear moduli of honeycombs with constant thickness cell walls.

By decomposing the cell walls into 5 blocks as shown in Fig. 6, the corresponding area of each block can be calculated as follow:

$$S_a = th_b \tag{B.1}$$

$$S_b = S_c = tl_b - 2S_e \tag{B.2}$$

$$S_d = \frac{t^2}{4\cos\theta}\left(2-\sin\theta\right) \tag{B.3}$$

$$S_e = \left[\frac{t}{2\cos\theta}\sqrt{\left(2-\sin\theta\right)^2 - 3cos^2\theta}\right]\left(\frac{t}{2}\right) = \frac{t^2}{4\cos\theta}\left(2\sin\theta - 1\right) \tag{B.4}$$

Assuming uniform stress field in block $d$ and $e$, compatibility of tractions at the interface of block $b$ and $e$ gives:

$$\tau_b = \tau_d \cos\theta = \tau_e \cos\theta \tag{B.5}$$

The equilibrium of forces in other directions requires that:

$$\tau_a = 0 \tag{B.6}$$

This has also been visualized in the contour plots of the stress field obtained from finite element simulation results (see Fig. 14(a)).

These blocks are made of the same material, therefore:

$$\gamma_b = \gamma_d \cos\theta = \gamma_e \cos\theta \tag{B.7}$$

Displacements at the inside edge of the inclined members should also be compatible with the overall displacement due to the overall shear strain $\gamma_{13}$. This can be written as:

$$2\gamma_b l_b = 2\gamma_{13} l_b \cos\theta \tag{B.8}$$

The equilibrium forces in the $X_1$ direction requires that the applied shear force $F_{13}$ on the unit cell be equal to the sum of shear forces that these block carries. i.e.:

$$\tau_b \cos\theta\left(tl_b - 2S_e\right) + S_d\tau_d + 2S_e\tau_e = \tau_{13}\left(l\cos\theta\right)\left(h + l\sin\theta\right) \tag{B.9}$$

Substituting Eqs. (B.1)-(B.5) into Eq. (B.9) gives the effective shear modulus as:

$$G_{13}^* = G_s\left(\frac{t/l}{\left(h/l+\sin\theta\right)\cos\theta}\right)\left[\left(\frac{l_b}{l}\right)\cos^2\theta + \frac{3}{4}\left(\frac{t}{l}\right)\tan\theta - \left(\frac{t}{l}\right)\frac{\cos\theta}{2}\left(2\sin\theta - 1\right)\right] \tag{B.10}$$

For shear loading in $X_2$-$X_3$ plane, again the applied shear stress induces shear forces in the cell wall blocks which should be in equilibrium with the applied shear force in $X_2$ direction, or:

$$\tau_b \sin\theta\left(tl_b - 2S_e\right) + S_d\tau_d + 2S_e\tau_e + \frac{S_a\tau_a}{2} = \tau_{23}\left(l\cos\theta\right)\left(h + l\sin\theta\right) \tag{B.11}$$

Again, assuming uniform stress field in block d and e, compatibility of tractions at the interface of block $b$ and $e$ gives:

$$\tau_b = \tau_d \sin\theta = \tau_e \sin\theta \tag{B.12}$$

$$\gamma_b = \gamma_d \sin\theta = \gamma_e \sin\theta \tag{B.13}$$

Compatibility of displacements along the outer edge of the cell walls requires:

$$\gamma_b l_b + h_b\gamma_a = \gamma_{23}\left(l_b \sin\theta + h_b\right) \tag{B.14}$$

Substituting Eqs. (B.12)-(B.14) into Eq. (B.11) gives the effective shear modulus as:

$$G_{23}^{*} = G_s\left(\frac{t/l}{\left(h/l + \sin\theta\right)\cos\theta}\right)\left[\frac{h_b}{2l} + \left(\frac{l_b}{l}\right)\sin^2\theta - \frac{1}{2}\left(\frac{t}{l}\right)\tan\theta\left(2\sin^2\theta - \sin\theta - \frac{3}{2}\right)\right] \tag{B.15}$$

It should be noted that the above equations for the effective out-of-plane shear moduli reduces to those given in (Gibson and Ashby, 1997) for regular Honeycombs (i.e. $h/l = 1$ and $\theta = 30^{\circ}$). In fact, at $\theta = 30^{\circ}$, $S_e = 0$ and the above equations can be simplified.

## Acknowledgments

Financial support from BASF through the North American Center for Research on Advanced Materials (Program Manager Dr. Marc Schroeder; Project Managers: Dr. Holger Ruckdaeschel and Dr. Rene Arbter) is gratefully acknowledged.

## References

ABAQUS Inc., 2013. ABAQUS analysis user's manual.

Allen, H.G., 1969. Analysis and design of structural sandwich panels, Analysis and Design of Structural Sandwich Panels. Elsevier.

Balawi, S., Abot, J.L., 2008. The effect of honeycomb relative density on its effective in-plane elastic moduli: An experimental study. Compos. Struct. 84, 293–299.

Bower, A.F., 2010. Applied mechanics of solids. CRC / Taylor & Francis, Boca Raton.

Burton, W.S., Noor, A.K., 1997. Assessment of continuum models for sandwich panel honeycomb cores. Comput. Methods Appl. Mech. Eng. 145, 341–360.

Catapano, A., Montemurro, M., 2014. A multi-scale approach for the optimum design of sandwich plates with honeycomb core. Part I: homogenisation of core properties. Compos. Struct. 118, 664–676.

Chamis, C.C., Aiello, R.A., Murthy, P.L.N., 1988. Fiber composite sandwich thermostructural behavior: computational simulation. J. Compos. Technol. Res. 10, 93–99.

Chen, D.H., 2011. Bending deformation of honeycomb consisting of regular hexagonal cells. Compos. Struct. 93, 736–746.

Gereke, T., Malekmohammadi, S., ASCE, S.M., Nadot-Martin, C., Dai, C., Ellyin, F., Vaziri, R., 2012. Multiscale Stochastic Modeling of the Elastic Properties of Strand-Based Wood Composites. J. Eng. Mech. 791–799.

Gereke, T., Malekmohammadi, S., Nadot-Martin, C., Dai, C., Ellyin, F., Vaziri, R., 2011. A numerical multiscale approach for stiffness predictions of wood composite, in: 26th ASC Annual Technical Conference (the Second Joint US--Canada Conference on Composites). Montreal.

Gibson, L.J., 1981. The elastic and plastic behaviour of cellular materials. University of Cambridge.

Gibson, L.J., Ashby, M.F., 1988. Cellular solids: structure and properties, First Edit. Pergamon Press, Oxford.

Gibson, L.J., Ashby, M.F., 1997. Cellular solids: structure and properties, Second Edi. Cambridge university press, New York.

Gibson, L.J., Ashby, M.F., Schajer, G.S., Robertson, C.I., 1982. The mechanics of two-dimensional cellular materials. Proc. R. Soc. A Math. Phys. Eng. Sci. 382, 25–42.

Grediac, M., 1993. A finite element study of the transverse shear in honeycomb cores. Int. J. Solids Struct. 30, 1777–1788.

Guedes, J., Kikuchi, N., 1990. Preprocessing and postprocessing for materials based on the homogenization method with adaptive finite element methods. Comput. Methods Appl. Mech. Eng. 83, 143–198.

Guo, X.E., Gibson, L.J., 1999. Behavior of intact and damaged honeycombs: a finite element study. Int. J. Mech. Sci. 41, 85–105.

Hexcel Corporation, 1999. HexWeb$^{TM}$ Honeycomb Attributes and Properties-A comprehensive guide to standard Hexcel honeycomb materials, configurations, and mechanical properties.

Hohe, J., Becker, W., 2001. A refined analysis of the effective elasticity tensor for general cellular sandwich cores. Int. J. Solids Struct. 38, 3689–3717.

Huet, C., 1990. Application of variational concepts to size effects in elastic heterogeneous bodies. J. Mech. Phys. Solids.

Kanit, T., Forest, S., Galliet, I., Mounoury, V., Jeulin, D., 2003. Determination of the size of the representative volume element for random composites: Statistical and numerical approach. Int. J. Solids Struct. 40, 3647–3679.

Kanit, T., N'Guyen, F., Forest, S., Jeulin, D., Reed, M., Singleton, S., 2006. Apparent and effective physical properties of heterogeneous materials: Representativity of samples of two materials from food industry. Comput. Methods Appl. Mech. Eng. 195, 3960–3982.

Karakoc, a, Freund, J., 2012. Experimental studies on mechanical properties of cellular structures using Nomex (R) honeycomb cores. Compos. Struct. 94, 2017–2024.

Kelsey, S., Gellatly, R.A., Clark, B.W., 1958. The shear modulus of foil honeycomb cores. Aircr. Eng. Aerosp. Technol. 30, 294–302.

Malekmohammadi, S., 2014. Efficient multi-scale modelling of viscoelastic composites with different microstructures. The University of British Columbia.

Masters, I.G., Evans, K.E., 1997. Models for the elastic deformation of honeycombs. Compos. Struct. 35, 403–422.

Meraghni, F., Desrumaux, F., Benzeggagh, M.L., 1999. Mechanical behaviour of cellular core for structural sandwich panels. Compos. Part A Appl. Sci. Manuf. 30, 767–779.

Michel, J.C., Moulinec, H., Suquet, P., 1999. Effective properties of composite materials with periodic microstructure: a computational approach. Comput. Methods Appl. Mech. Eng. 172, 109–143.

Moulinec, H., Suquet, P., 1998. A numerical method for computing the overall response of nonlinear composites with complex microstructure. Comput. Methods Appl. Mech. Eng. 157, 69–94.

Python, 2013. The Python Language Reference.

Qing, H., Mishnaevsky, L., 2009. 3D hierarchical computational model of wood as a cellular material with fibril reinforced, heterogeneous multiple layers. Mech. Mater. 41, 1034–1049.

Silva, M.J., Hayes, W.C., Gibson, L.J., 1995. The effects of non-periodic microstructure on the elastic properties of two-dimensional cellular solids. Int. J. Mech. Sci. 37, 1161–1177.

Simone, A.E., Gibson, L.J., 1998. Effects of solid distribution on the stiffness and strength of metallic foams. Acta Mater. 46, 2139–2150.

Timoshenko, S., Goodier, J.N., 1970. Theory of Elasticity, third. ed. McGraw-Hill, Tokyo.

Vougiouka, G., Rodrigues, H., Guedes, J.M., 1998. Prediction of elastic properties of sandwich panels using a homogenization computational model, in: Mechanics of Sandwich Structures. Springer, pp. 147–154.

Wang, C.M., Reddy, J.N., Lee, K.H., 2000. Shear Deformable Beams and Plates, Shear Deformable Beams and Plates. Elsevier, Oxford.

Xia, Z., Zhang, Y., Ellyin, F., 2003. A unified periodical boundary conditions for representative volume elements of composites and applications. Int. J. Solids Struct. 40, 1907–1921.

Zhang, J., Ashby, M.F., 1992. The out-of-plane properties of honeycombs. Int. J. Mech. Sci. 34, 475–489.

**Figures**

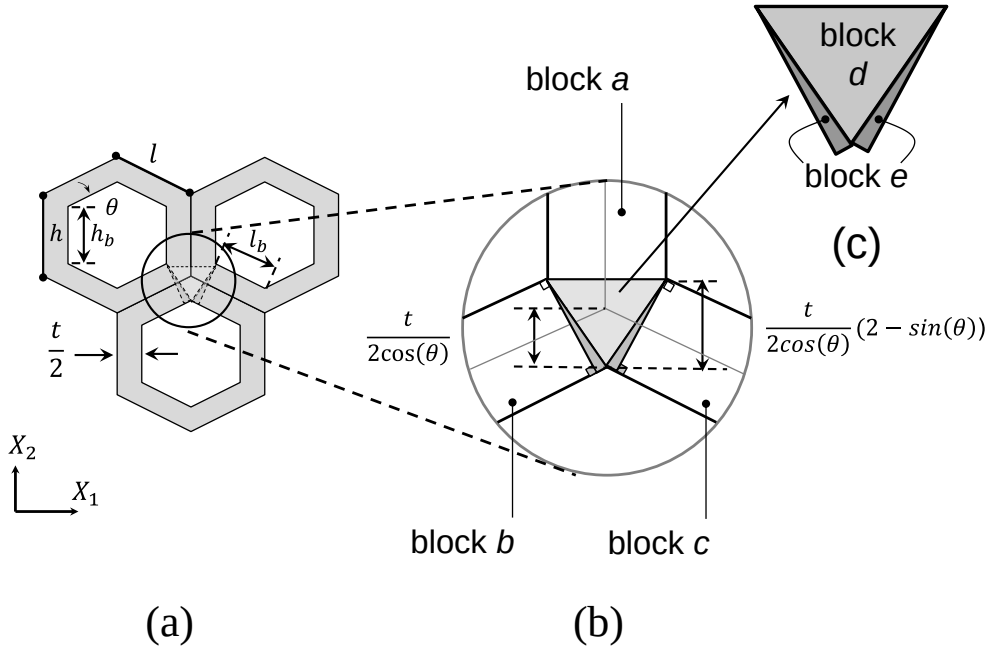


Fig. 1 Effective bending lengths of the cell wall, $l_b$ and $h_b$, for periodic hexagonal honeycombs with uniform wall thickness. Schematic representation of (a) honeycomb cells, (b) geometrical dimensions and (c) building blocks of the node region.

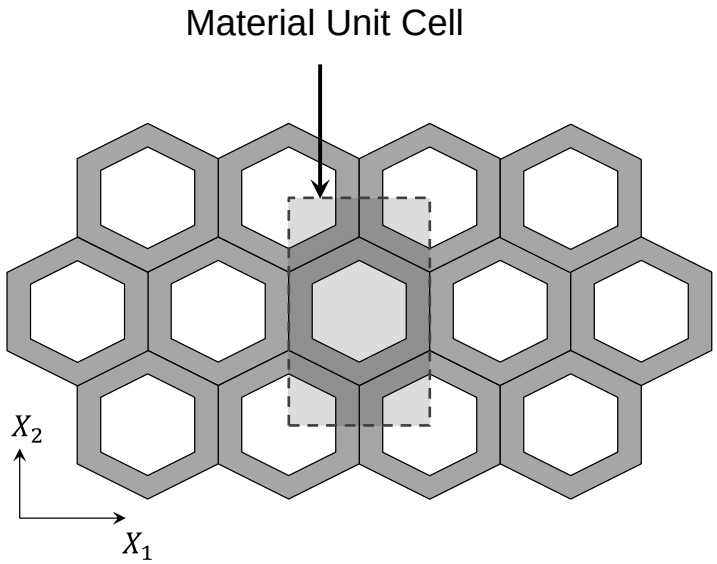


Fig. 2 Schematic representation of periodic, hexagonal honeycombs. A unit cell of the material has been highlighted.

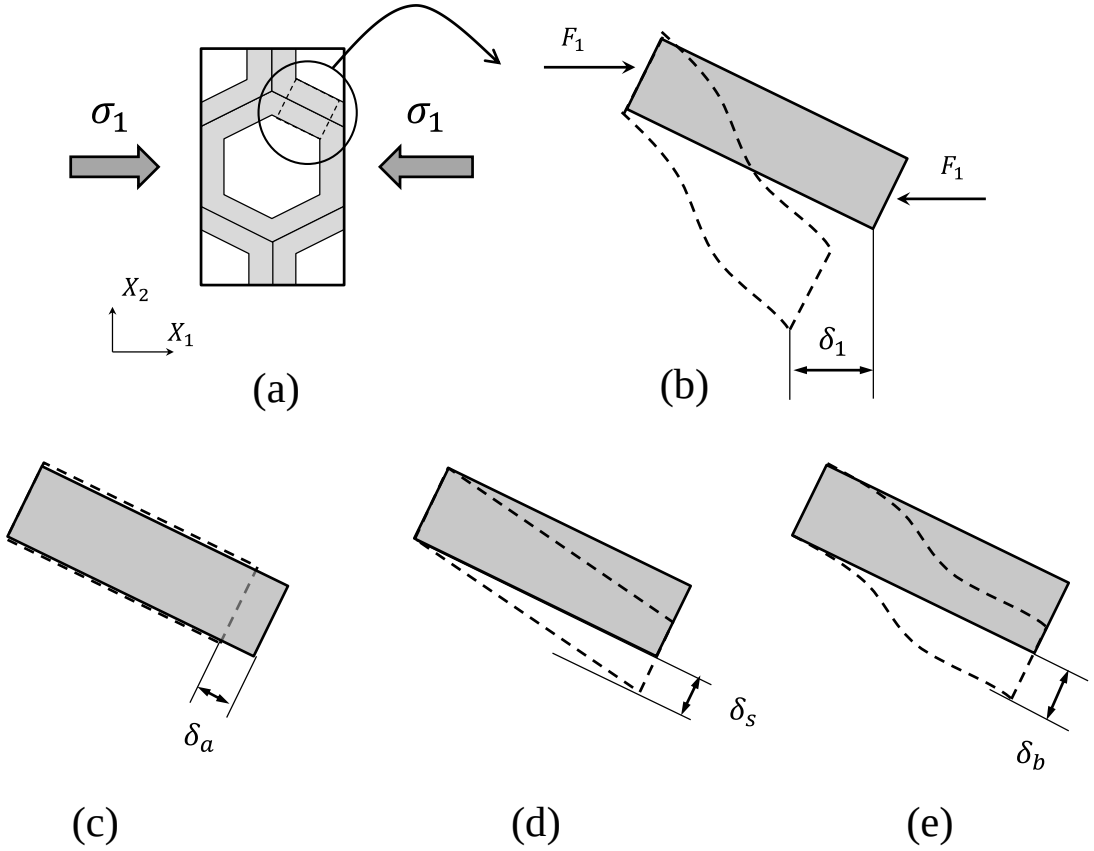


Fig. 3 Hexagonal honeycombs under in-plane loading in the $X_1$ direction: (a) unit cell of the material. Schematic representation of (b) the deformed shape and the deflections in the inclined member due to (c) axial, (d) shear and (e) bending deformations.

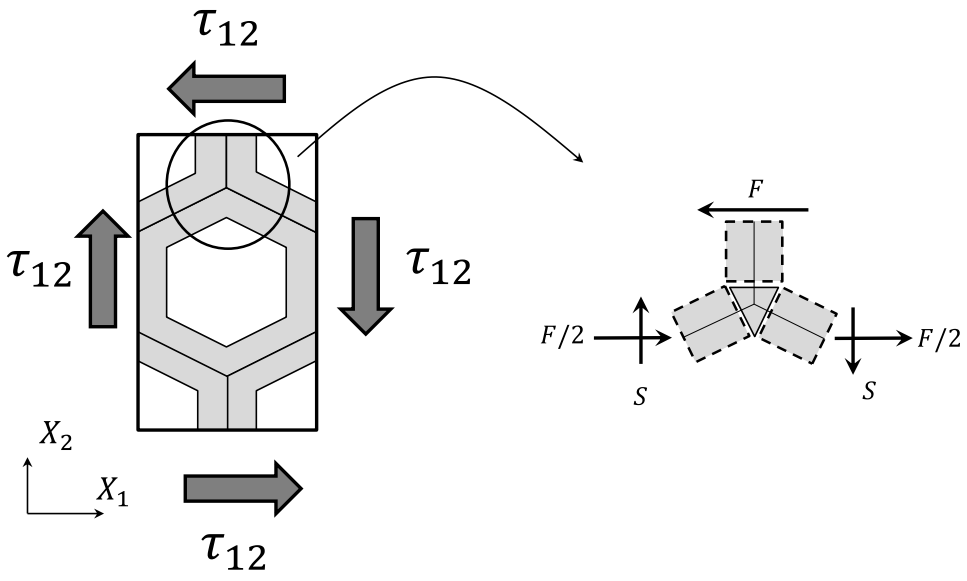


(a) (b)

Fig. 4 Hexagonal honeycombs under in-plane shear loading: (a) unit cell of the material, (b) loads acting on the vertical and inclined members.

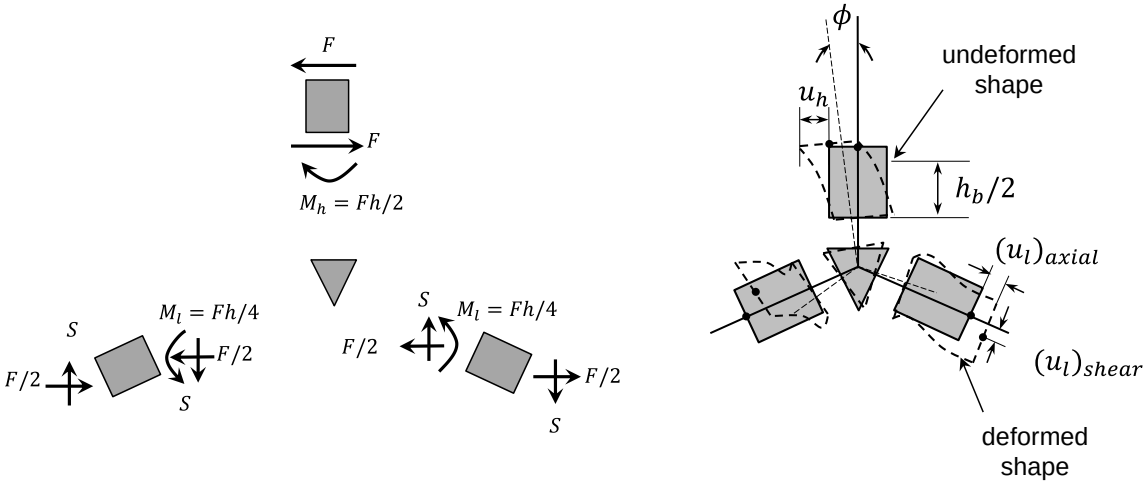


(a) (b)

Fig. 5 Hexagonal honeycombs under in-plane shear loading: (a) equilibrium of the cell walls under in-plane shear loading, (b) deflections of the vertical member ($u_h$) and the inclined

member ($u_l$) due to axial, bending and shear deformations. The undeformed and deformed shape of the members is shown in thick solid lines and dashed lines, respectively.

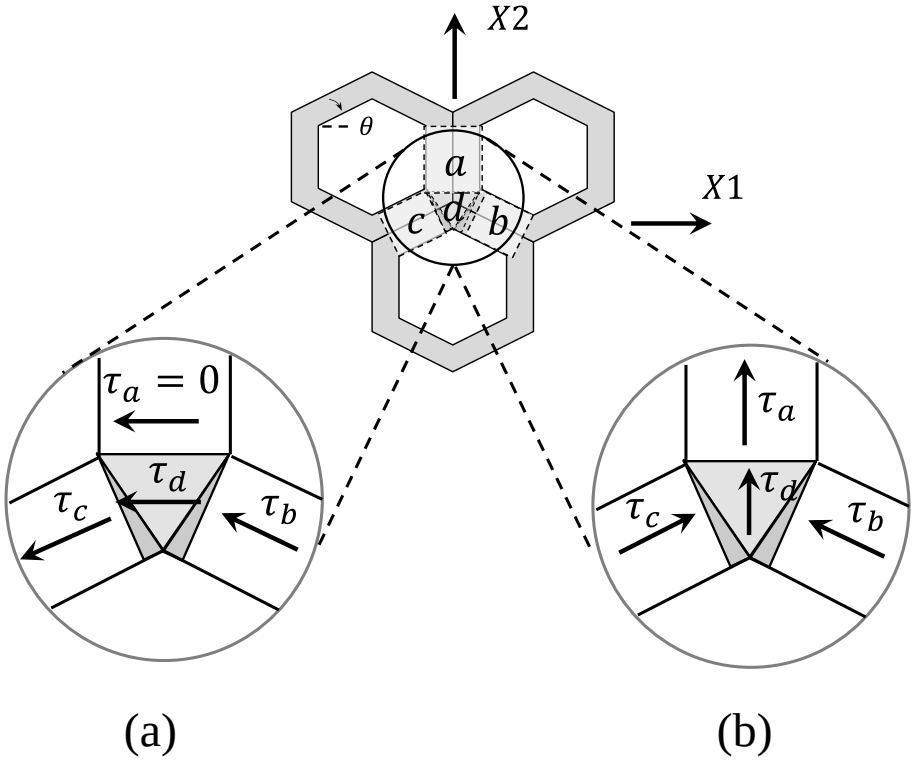


Fig. 6 Schematic representation of the assumed shear stress distributions in the honeycomb cell walls when loaded in the (a) $X_1 - X_3$ and (b) $X_2 - X_3$ plane.

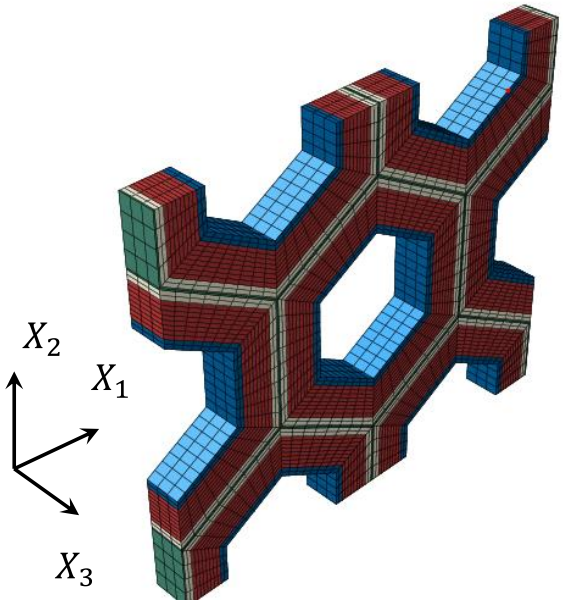


Fig. 7 Discretized unit cell of the honeycomb structure. The different colours represent the different layers in wood cell wall (CML, S1, S2 and S3)

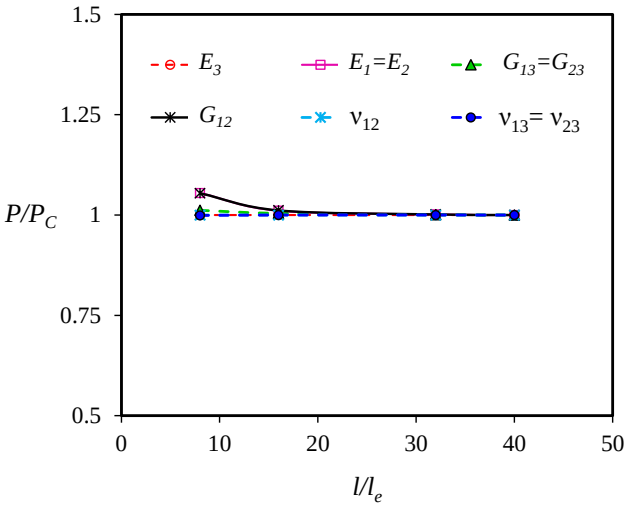


Fig. 8 Convergence study on the effective engineering constants of a regular honeycomb with constant cell wall thickness ( $\rho^* / \rho_s = 0.018$ ). The vertical axis shows the values of the effective properties ( $P$ ) normalized by their converged values ( $P_C$ ). The horizontal axis indicates the number of elements along each inclined member (see Fig. 7). A similar study was performed for the cell wall thickness and depth.

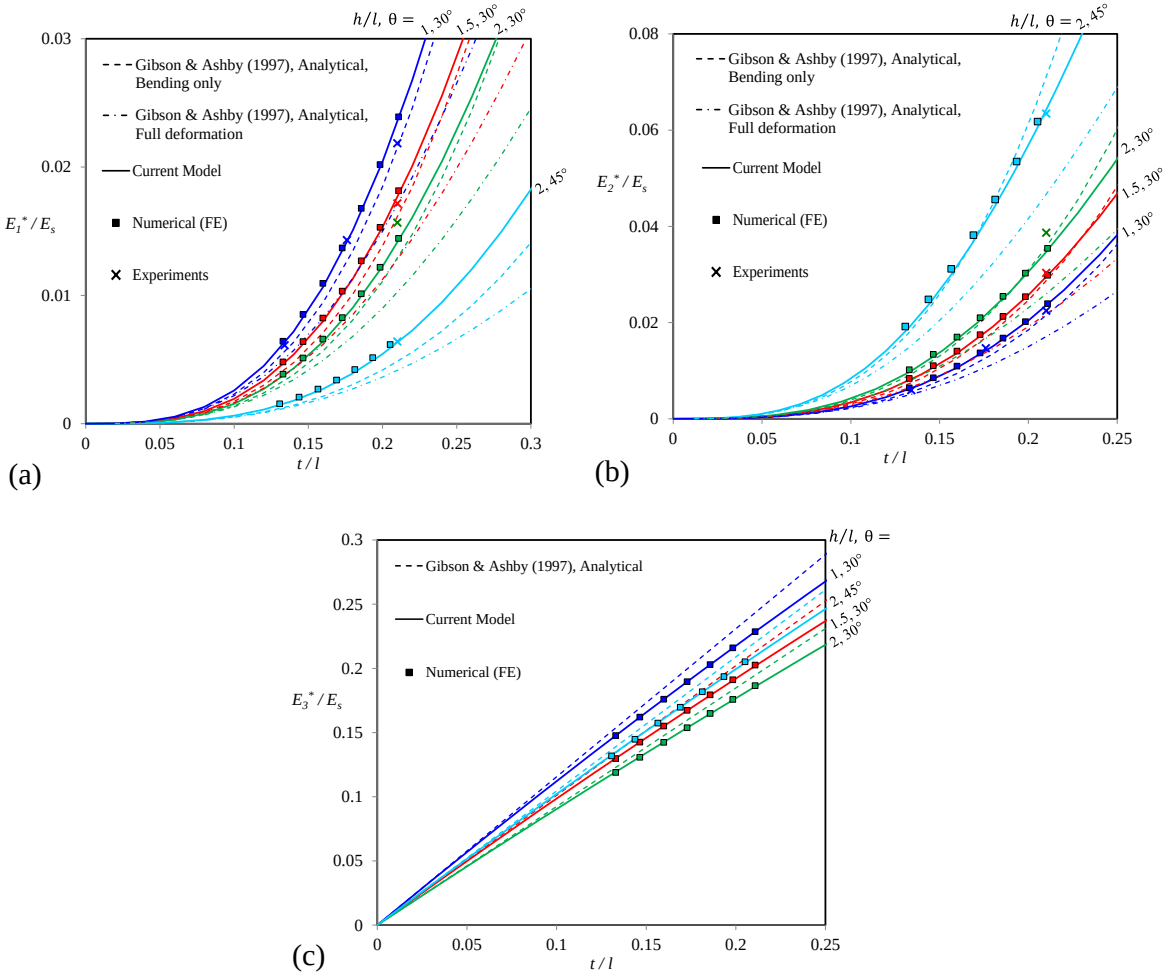


Fig. 9 Effective Young's modulus in the (a) $X_1$, (b) $X_2$ and (c) $X_3$ directions. Comparisons between analytical model predictions of Gibson and Ashby (1997) shown by dashed (bending deformations only) and dotted-dashed (axial, shear and bending deformations) lines, current analytical model (Eqs. 3, 11 and 12) shown by solid lines, numerical (FE) results shown by square symbols, and experimental data (Gibson 1981) shown by crosses. Predictions are given for different cell wall geometries.

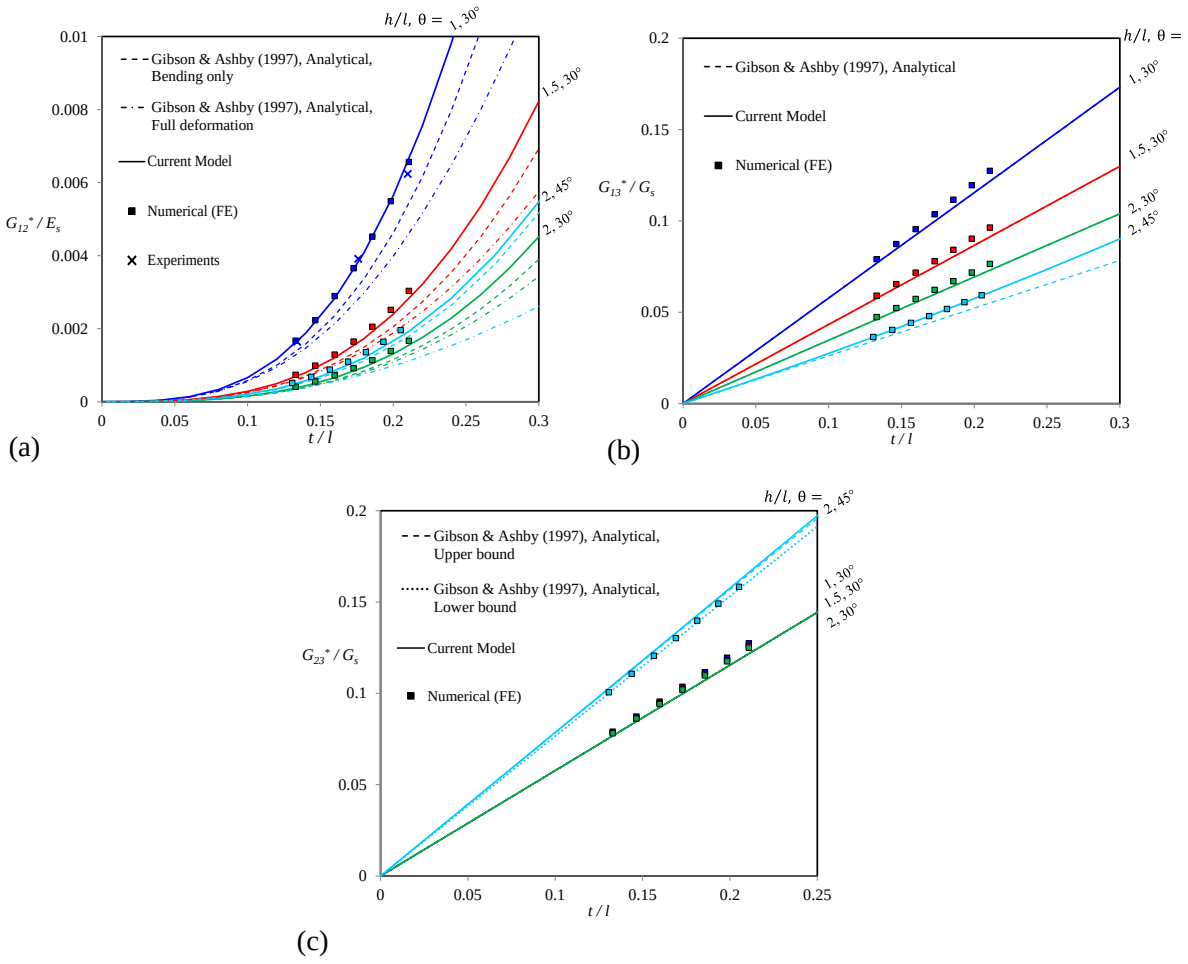


Fig. 10 Effective shear modulus in the (a) $X_1 - X_2$, (b) $X_1 - X_3$, and (c) $X_2 - X_3$ planes. Comparisons between analytical model predictions of Gibson and Ashby (1997) shown by dashed (bending deformations only) and dotted-dashed (axial, shear and bending deformations) lines, current analytical model (Eqs. 24, 26 and 27) shown by solid lines, numerical (FE) results shown by square symbols, and experimental data (Gibson 1981) shown by crosses. Predictions are given for different cell wall geometries.

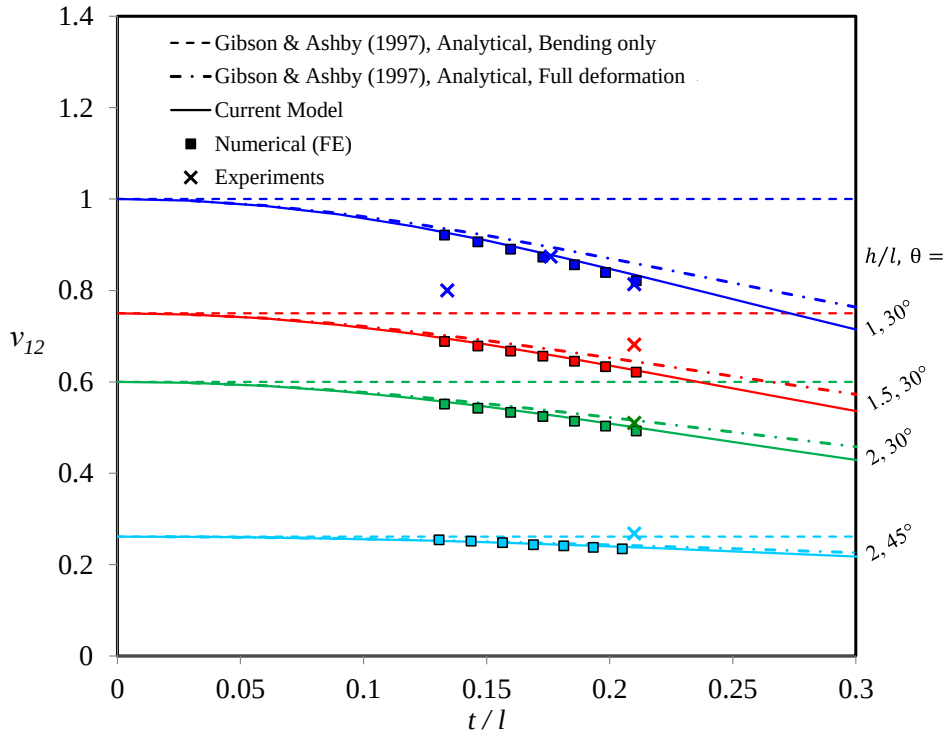


Fig. 11 Effective in-plane Poisson's ratio. Comparisons between analytical model predictions of Gibson and Ashby (1997) shown by dashed (bending deformations only) and dotted-dashed (axial, shear and bending deformations included) lines, current analytical model (Eq. 13) shown by solid lines, numerical (FE) results shown by square symbols, and experimental data (Gibson 1981) shown by crosses. Predictions are given for different cell wall geometries.

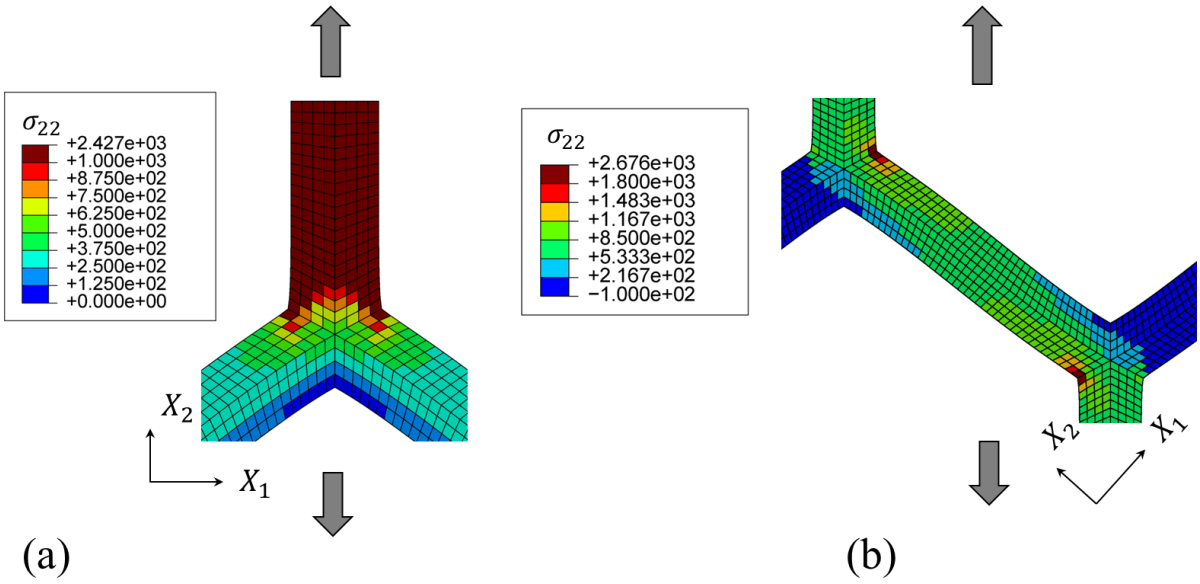


Fig. 12 Stress distribution in a regular honeycomb under tensile loading in the $X_2$ direction: (a) vertical member, (b) inclined member.

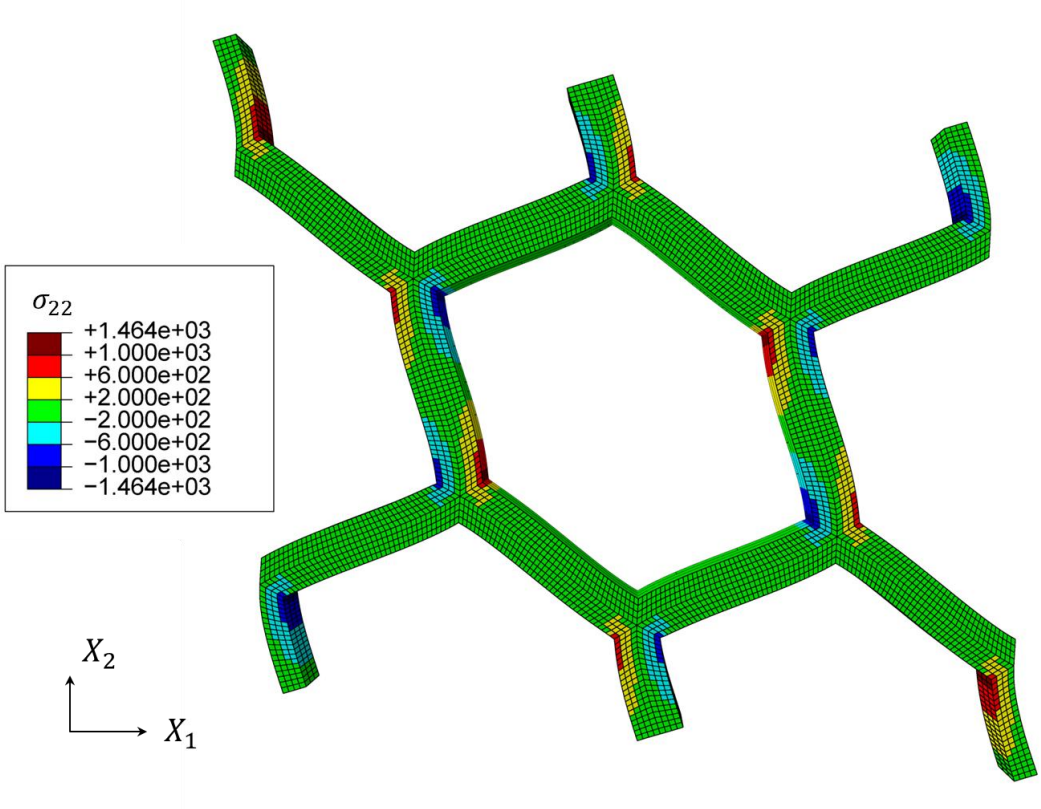


Fig. 13 Stress distribution in a regular honeycomb under in-plane shear loading.

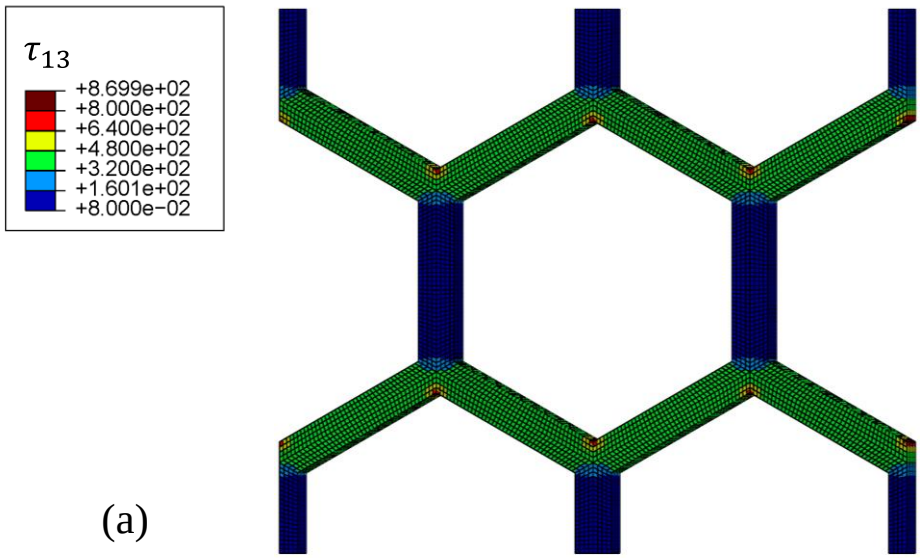


(a)

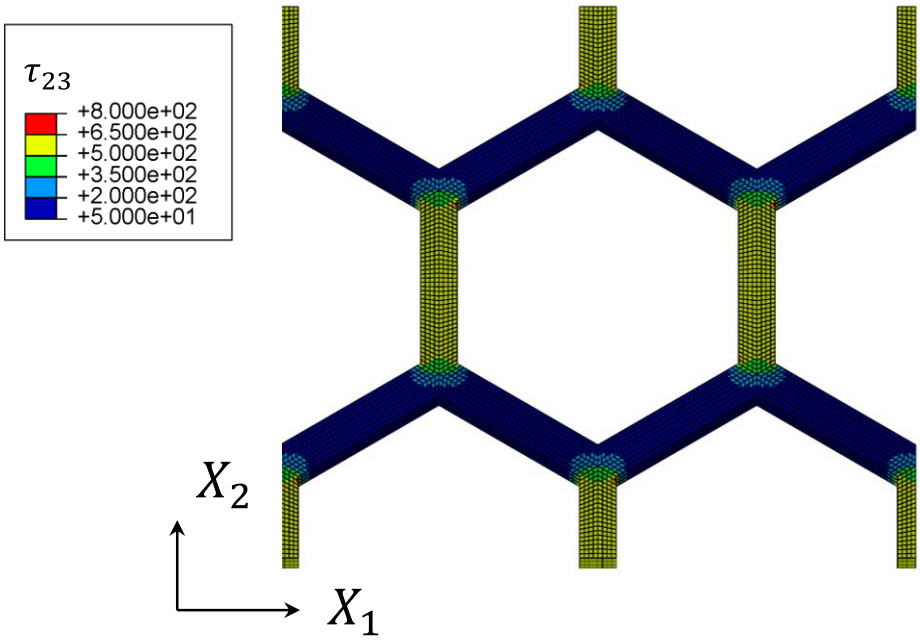


(b)

Fig. 14 Stress distribution in a regular honeycomb under out-of-plane shear loading when loaded in: (a) $X_1 - X_3$ plane, (b) $X_2 - X_3$ plane.

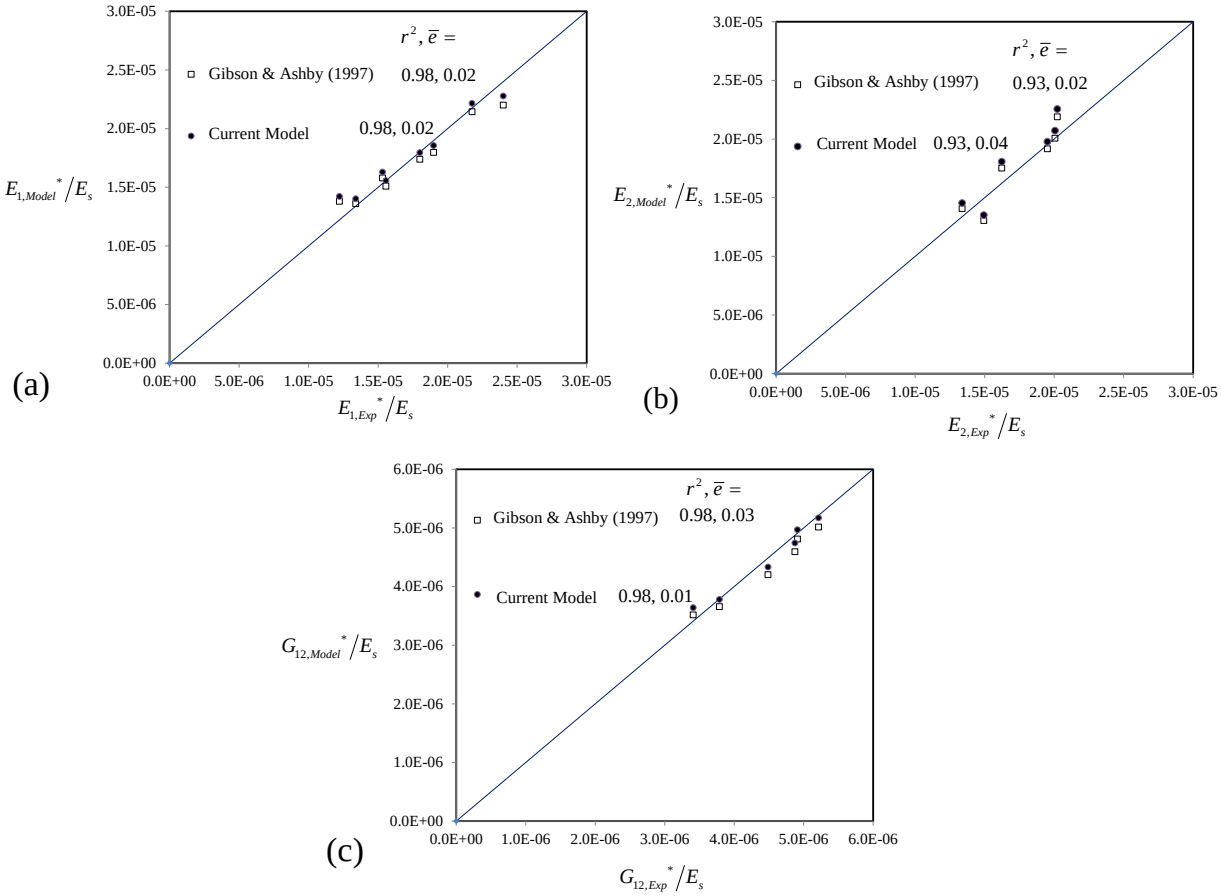


Fig. 15 Effective in-plane properties of honeycombs with double thickness vertical cell walls. Comparisons between the model predictions (previous analytical model (Gibson and Ashby 1997) and current analytical model (Eqs. A.4-A.6)) and experimental data (Karakoç and Freund (2012)) for the effective (a) Young's modulus in $X_1$ direction, (b) Young's modulus in $X_2$ direction and (c) shear modulus in $X_1 - X_2$ plane. The correlation coefficient, $r^2$, and the relative error, $\bar{e}$, between the predictions and experimental data are given for each property.

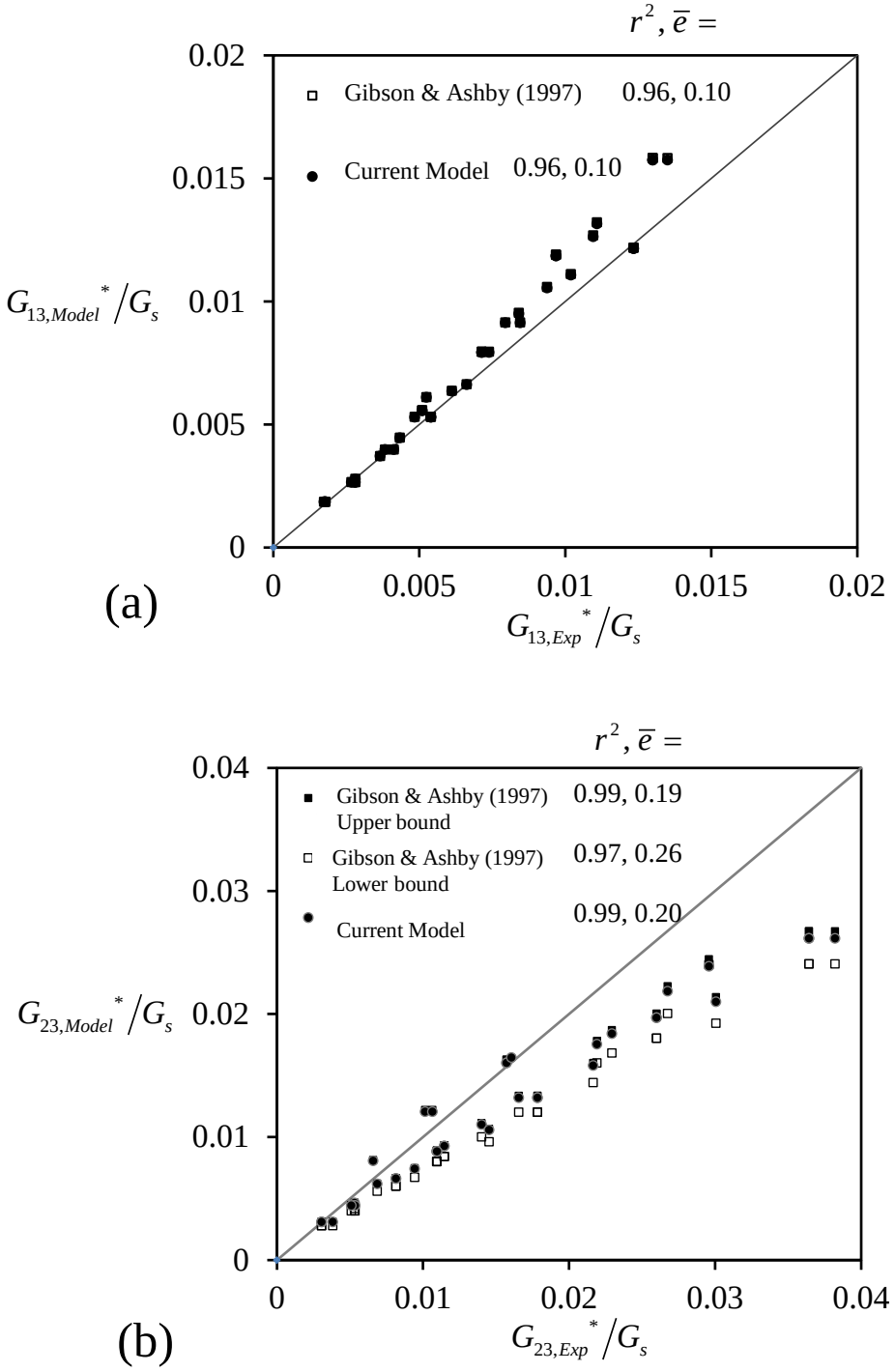


Fig. 16 Effective out-of-plane shear properties of honeycombs with double thickness vertical cell walls. Comparisons between the model predictions (previous analytical model (Gibson and Ashby 1997) and current analytical model (Eqs. A.7 and A.8)) and experimental data (Hexcel 1999) for the effective shear modulus in (a) $X_1 - X_3$ and (b) $X_2 - X_3$ plane. The correlation coefficient, $r^2$, and the relative error, $\bar{e}$, between the predictions and experimental data are given for each property.

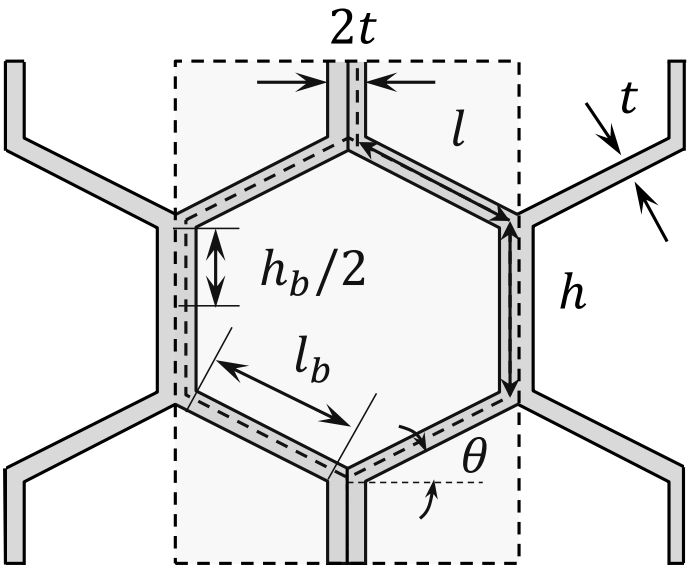


Fig. A1 Geometrical parameters defined for honeycombs with double thickness vertical cell walls.